Journal of Alloys and Compounds, 203 (1994) 117–126
JALCOM 902

Solid state nitrization reaction of amorphous tantalum aluminium nitride alloy powders: the role of amorphization by reactive ball milling

M. Sherif El-Eskandarany
Mining and Petroleum Engineering Department, Faculty of Engineering, Al-Azhar University, Nasr City, Cairo (Egypt)

(Received June 8, 1993)

Abstract

Amorphous tantalum aluminium nitride alloy powders have been synthesized by high energy ball milling under a purified nitrogen gas (N_2) flow at room temperature. The modes of amorphization and crystallization of the TaAlN alloy powders have been investigated by means of X-ray diffraction, optical metallography, scanning electron microscopy, transmission electron microscopy and differential thermal analysis. The mechanical alloying process via the reactive ball-milling technique is classified into three stages of milling. During the first stage the elemental powders of Ta and Al particles grow in size to form layered composite particles of larger diameter as a result of cold welding. In the second stage the elemental Al powders completely diffuse into the Ta matrix to form a b.c.c. TaAl solid solution. This solid solution expands with increasing the milling time to give a saturation value of the lattice parameter a_0 of 0.3306 nm after 55 ks of milling. At this stage the powders are disintegrated into several particles which have new or fresh surfaces that are able to absorb nitrogen gas, so that both the b.c.c. TaAl solid solution and the unprocessed b.c.c. Ta powder particles react with nitrogen to form a b.c.c. TaAl solid solution nitride and h.c.p. TaN respectively. Further milling creates mechanical deformations such as point defects and dislocations which lead to an increase in the free energy of the nitride phase of the b.c.c. TaAl solid solution to the less stable phase of amorphous TaAlN. In addition, solid state amorphization reactions between h.c.p. TaN and the b.c.c. TaAl solid solution occur. During the final stage of milling (72 ks) a homogeneous phase of amorphous TaAlN is formed containing 18 at.% N_2. The crystallization characteristics represented by the crystallization temperature T_x and the enthalpy change of crystallization, ΔH_x, are 1115 K and -95 kJ mol^{-1} respectively.

1. Introduction

Fundamentally, the term milling may be defined as the breaking down of a relatively coarse material to its ultimate fineness. The milling process has been used via the ball-milling technique for the comminution of ores and the preparation of materials for industrial applications, *e.g.* grinding of iron ore for the preparation of pellets, grinding of talc to prepare body powder, etc.

Apart from the grinding of ores for their subsequent beneficiation, Benjamin [1] employed the ball-milling technique to produce homogeneous composite particles with an intimately dispersed, uniform internal structure by a process called mechanical alloying (MA). Since then the MA process has been used for preparing many dispersion-strengthened alloy powders [2–4].

Ten years ago Koch *et al.* [5] reported the first novel technique of amorphization by MA of elemental powders of Ni and Nb using a high energy ball mill. The mechanism of amorphization by ball milling is believed to be analogous to that of amorphization by the solid state amorphization reaction (SSAR) [6] method. Comparable with the MA process, amorphous alloys can be prepared by grinding the crystalline compound, *i.e.* mechanical grinding (MG) [7] or mechanical disordering (MD) [8].

In fact, the MA process via the ball-milling technique has been considered as a practical solution for amorphizing systems which are difficult or impossible to obtain by conventional melting techniques, *e.g.* Al–Ta [9] and Al–Nb [10, 11] binary systems. It has also been used for the amorphization of systems exhibiting a positive heat of mixing [12, 13]. Moreover, it has been shown by Gaffet and Harmelin [14] that amorphous silicon powder can be obtained by milling elemental silicon powder under purified argon gas in a ball mill.

In 1990 Sherif El-Eskandarany *et al.* [15] reported a novel technique for producing amorphous $Al_{30}Ta_{70}$ alloy powders from pure aluminium and tantalum powders by rod milling. This unique technique has been

SSDI 0925-8388(93)00902-B

accepted as a successful method for producing amorphous alloy powders with a low degree of contamination, *i.e.* iron contamination, and high thermal stability through the SSAR method. The application of this new technique has led to the formation of many amorphous alloy powders [16–22]. Within the last few years a lot of research activity has concentrated on the formation of amorphous and/or compound alloy powders by the MA process [23–27].

We should say that the MA process is more than just a unique method for preparing amorphous alloys. It is also a unique technique for preparing several metal nitrides [28–31] using a method called reactive ball milling (RBM) [29].

In the present study we have utilized X-ray diffraction, scanning electron microscopy and transmission electron microscopy to monitor the crystal-to-amorphous phase transition in TaAlN alloy powders prepared by the RBM technique. The crystallization characteristics and thermal stability of amorphous TaAlN alloy were investigated by differential thermal analysis. The mechanism of synthesis of amorphous TaAlN alloy via RBM will be discussed. Further, there was the desire to make morphological and calorimetric studies of a new metallic amorphous nitride system for which there is no information and thermodynamic data.

2. Experimental procedures

In the present study we have used high purity elemental powders of Ta (99.999%, 50 μm) and Al (99.99%, 50 μm) and high purity nitrogen and argon gases (H_2O and O_2 less than 5 ppm) as starting materials. A high energy vibrating ball mill equipped with a rotary pump and a gas flow system has been used in the present work. Before starting the RBM process, the elemental Ta and Al powders were balanced and mixed in a glove-box under a purified Ar atmosphere to give the nominal composition $Ta_{50}Al_{50}$. The mixed powders were charged and sealed in a sapphire vial (80 ml in volume) together with 15 sapphire balls of 11 mm in diameter under purified argon gas. The ball-to-powder weight ratio was controlled to be 7:1. The vial was mounted on the mill and evacuated for about 5 ks. Then a flow of nitrogen gas (0.80 ml s^{-1}) was passed through the inlet of the vial via a plastic pipe. The outlet of the vial was connected to an oil bubbler. Once gas bubbles were observed, the milling process was started at a frequency of about 11 Hz. The gas was continuously introduced at a rate of 1.00 ml s^{-1}. The milling process was stopped at regular intervals and a small amount of powder removed from the vial in the glove-box.

The alloy powders were characterized by X-ray diffraction (XRD) with Cu Kα radiation, optical metallography, scanning electron microscopy (SEM) operating at 25 kV and transmission electron microscopy (TEM) with a 200 kV microscope. However, high resolution transmission electron microscopy (HRTEM) with a 1 MV microscope has been used for the characterization of some mechanically alloyed powders. The crystallization properties and thermal stability of the amorphous TaAlN alloy powders have been determined by means of differential thermal analysis (DTA) under an argon gas atmosphere at a heating rate of 0.33 K s^{-1}. The DTA was calibrated using metallic Sn, Zn, Pb, Al, Ag and Au. Moreover, well-known amorphous alloy ribbons such as NiZr were used in the calibration as well. For the DTA experiments a sample (about 50 mg) of the milled powder was inserted in a platinum pan and then the system was evacuated for about 5 ks using a rotary pump for 1 ks and a diffusion pump for 4 ks. A certain amount of α-Al_2O_3 powder (about 60 mg) was put into the platinum reference pan and the lining of the sample platinum pan was coated with α-Al_2O_3 powder to avoid any reactions between the sample (especially tantalum) and the platinum pan which could give false exothermic peak(s) especially at elevated temperatures. In addition, the level of oxygen contamination and the nitrogen gas content in the milled alloy powders were determined by the induction helium carrier fusion–thermal conductivity method. At the final stage of milling the oxygen and nitrogen contents were 0.70 and 18 at.% respectively. Since we have used a sapphire milling medium, the common problem of iron contamination in the end-product alloy powders could be overcome. Moreover, no foreign materials such as Zr could be detected in the alloy powders using inductively coupled plasma (ICP) analysis.

3. Results

3.1. Structural change with milling time

X-ray analyses were performed in order to understand the structure of the mechanically alloyed powders during the RBM process. Figure 1 presents the XRD patterns of $Ta_{50}Al_{50}$ alloy powders after selected RBM times. After 43 ks of RBM all the Bragg peaks for crystalline f.c.c. Al have completely disappeared. In addition, the Bragg peaks for crystalline b.c.c. Ta have become broader and their positions have shifted markedly to the low angle side, indicating the formation of a b.c.c. TaAl solid solution. It is worth noting that after 55 ks of RBM these peaks become broader with diffuse haloes, suggesting the formation of an amorphous phase coexisting with the b.c.c. TaAl solid solution, as shown

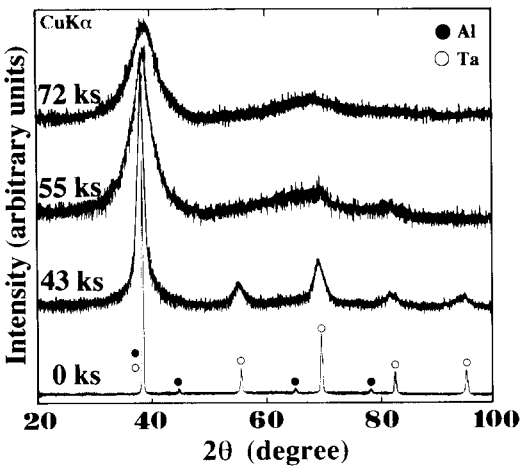

Fig. 1. Typical XRD patterns of TaAlN alloy powders after various RBM times.

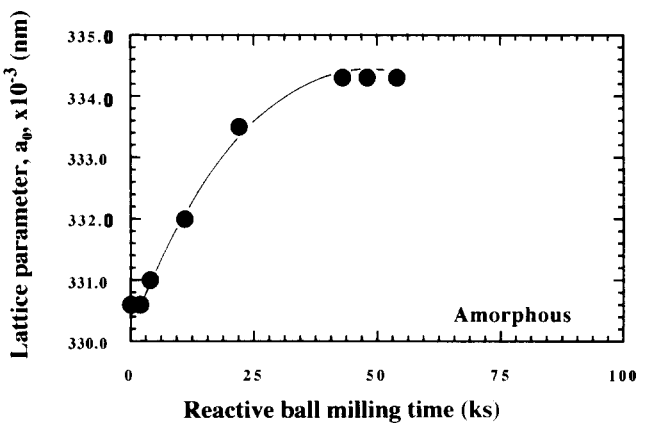

Fig. 2. Effect of progressive RBM time on the lattice parameter a_0 of TaAlN alloy powders.

in Fig. 1. At the final stage of RBM (72 ks) the b.c.c. TaAl solid solution phase has been completely transformed to a homogeneous amorphous phase characterized by diffuse haloes and smooth peaks. We should emphasize that this amorphous phase does not change to any other phase(s) even for samples milled for times as long as 96 ks.

The lattice parameter a_0 of mechanically alloyed $Ta_{50}Al_{50}$ powders estimated from XRD measurements is shown in Fig. 2 as a function of the RBM time. Obviously the b.c.c. TaAl solid solution expands with increasing RBM time, as characterized by a monotonic increase in a_0 to give a saturation value of 0.3343 nm after 43 ks of RBM. This value is larger than that of pure crystalline Ta (0.3306 nm), suggesting an interstitial solubility of Al in Ta. This value does not change with further milling (55 ks), indicating the formation of a saturated solid solution.

3.2. Morphology and metallography changes with milling time

The SEM technique was used to follow the changes in size and shape of mechanically alloyed $Ta_{50}Al_{50}$ powders milled under a flow of nitrogen for various RBM times. Detailed SEM observations after several stages of the RBM process are presented in Fig. 3. After a few kiloseconds of RBM the starting elemental powders of Ta and Al (about 60 μm in diameter) have agglomerated to form composite particles about 400 μm in diameter with a plate-like morphology (Fig. 3a). After 22 ks of RBM the powder particles have decreased in size (100 μm in diameter) and exhibit an extremely rough surface relief (Fig. 3b). These particles of flake-cabbage or flake-orange skin-like morphology contain many narrow layers of Ta and Al in a well-ordered arrangement and each layer has a width of about 5 μm or less (Fig. 4a). During the progress of RBM the assemblage particles have continuously disintegrated to form powder particles which are irregular in shape (globe- and flake-like morphologies) and size (10–40 μm) (Fig. 3c). Optical metallography examination of the cross-section of polished and etched particles after this stage of milling shows that the layered structure morphology has already disappeared and that individual particles have no details on their polished surfaces (Fig. 4b). At the end of the RBM process (86 ks) the powder particles are fairly uniform in size, varying only from 0.5 to 1 μm in diameter. Moreover, the end-product of TaAlN alloy powder has a smooth sphere-like morphology without any relief details on the surface (Fig. 3d).

Figure 5 summarizes the SEM observations of mechanically alloyed $Ta_{50}Al_{50}$ powders milled under a flow of nitrogen for various RBM times. Obviously the MA process performed by the RBM technique can be classified into three stages, *i.e.* early, intermediate and final stages. In the early stage (0–22 ks) the elemental powders of Ta and Al have agglomerated and grown in size as a result of the repeated cold welding. During this stage of RBM the powders vary widely in size from 150 to 500 μm. During the subsequent intermediate stage (22–55 ks) the agglomerated powder particles are subjected to continuous disintegration with fragmentation to form finer powders less than 10 μm in diameter. Furthermore, this stage of milling produces powder particles with a narrow size distribution (Fig. 5). The final stage (55–86 ks) relates to the last stage of RBM in which all the powders are uniform and homogeneous in shape and size. In addition, this stage of milling gives powders as fine as 1 μm in diameter.

Since SEM and optical microscopy observations are not able to give any information about the structure of the phase(s) formed during the RBM process, detailed TEM analyses were performed in order to observe the

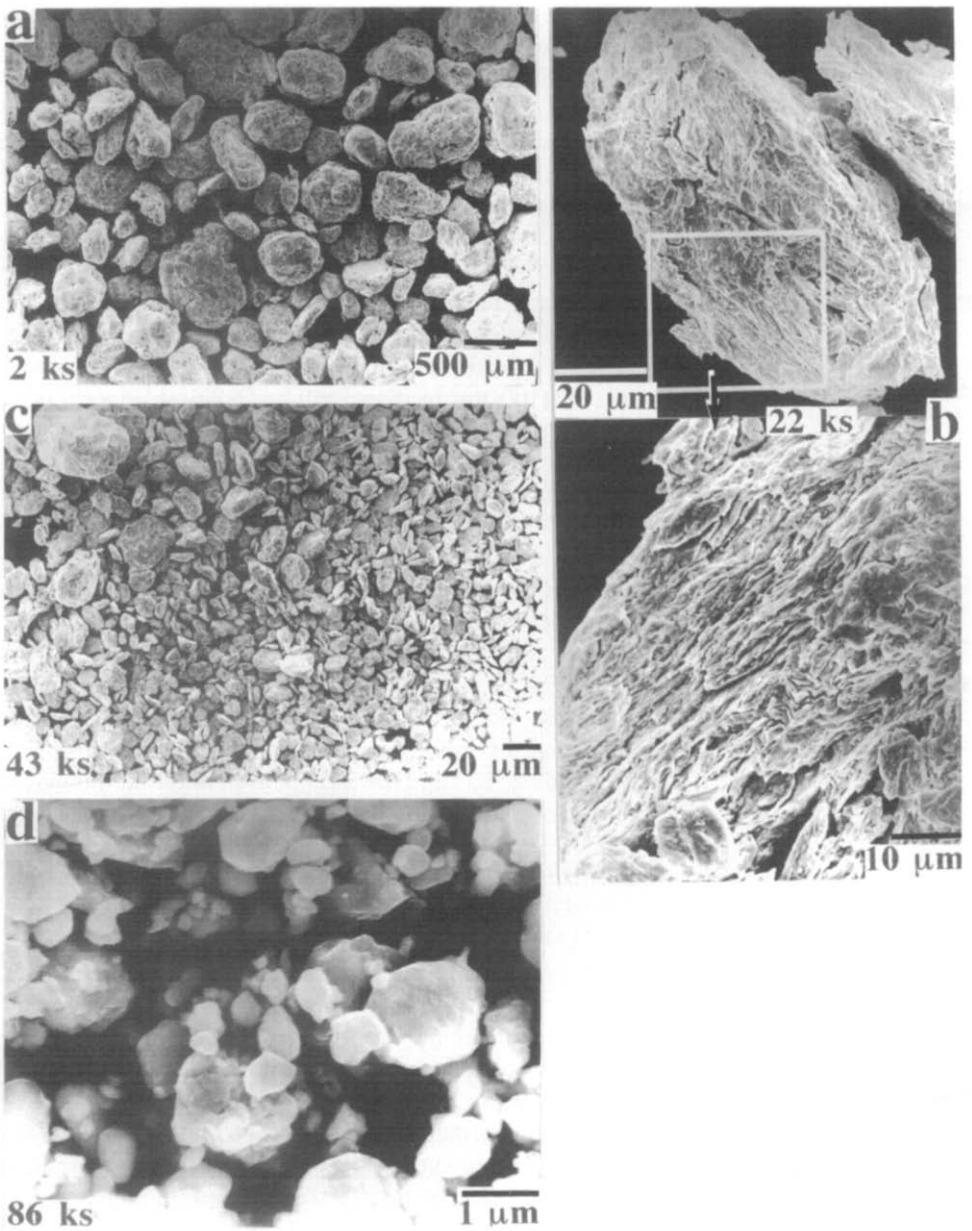

Fig. 3. SEM images of TaAlN alloy powders milled for RBM times of (a) 2 ks, (b) 22 ks, (c) 43 ks and (d) 86 ks.

structural changes in the mechanically alloyed TaAlN powder particles during the above-mentioned stages of milling. The bright field images (BFIs) and/or dark field images (DFIs) and the selected area diffraction patterns (SADPs) of mechanically alloyed TaAlN powder particles after various RBM times are shown in Fig. 6. Figure 6a shows the BFI and corresponding SADP of powder particles taken after 2 ks of RBM. The powder is a mixture of polycrystalline Ta and Al with grain boundary fringes and dislocations in the boundary. The SADP taken at the centre of the micrograph shows a sharp spot pattern related to b.c.c. Ta coexisting with f.c.c. Al (inset of Fig. 6a). Increasing the RBM time leads to greater impact shear forces being generated by the balls and this causes mechanical deformation of the powder particles. Numerous faults and dislocations appear clearly in the micrograph of the particles taken after 22 ks of milling (Fig. 6b). The oriented particles have twin and nanotwin boundaries on Al(111) and Ta(110) planes as shown in the corresponding SADPs of zones I and II respectively. Moreover, several defects with grain boundary movement are clearly seen near the centre of the micrograph.

The DFI has been used in order to determine the crystalline size of the alloy powders in a direct way. Figure 6c shows the DFI and corresponding SADP of the TaAlN powder at the mid-interval RBM process time. The powder particles have a cell-like morphology

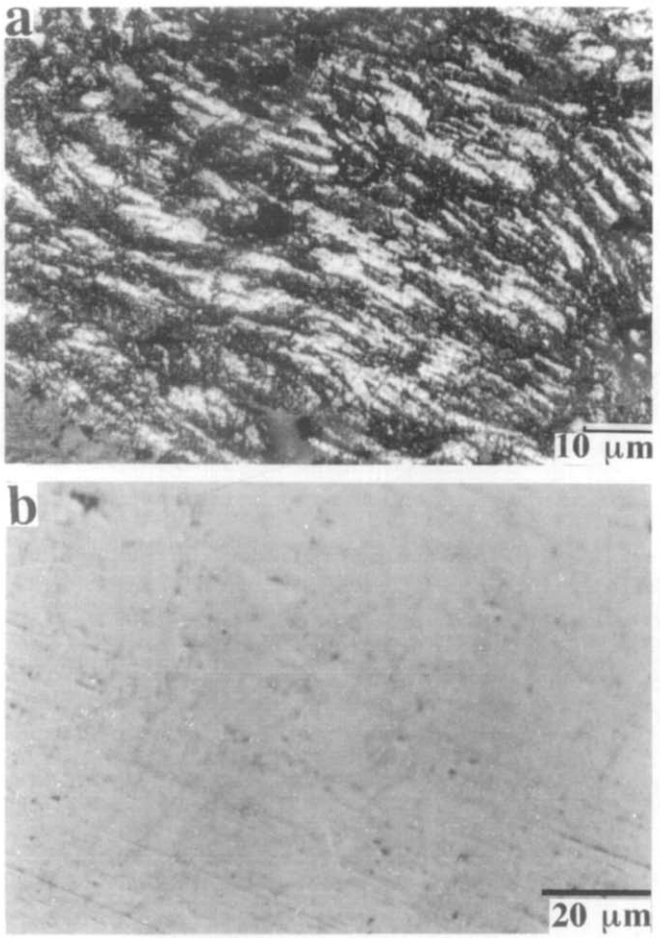

Fig. 4. Optical micrographs of polished surface of TaAlN alloy powders milled for RBM times of (a) 22 ks and (b) 55 ks.

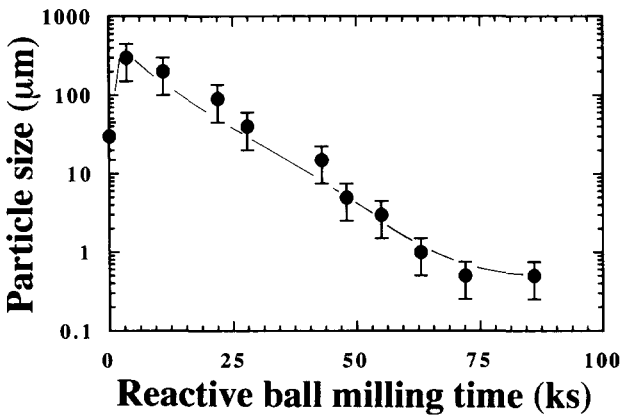

Fig. 5. Effect of progressive RBM time on particle size distribution of TaAlN alloy powders.

containing very fine grains with nanodimensions (about 10 nm or less in diameter). The Debye–Scherrer rings of the SADP show the formation of a b.c.c. TaAl solid solution coexisting with unprocessed Ta and/or Al (small spots) (inset of Fig. 6c).

Figure 6d shows the BFI of the TaAlN alloy powder after 55 ks of RBM. It is worth noting that the structure of the overall matrix is amorphous (fine structure), containing several phases, as shown by the different features of the SADPs taken from various regions. The BFI is classified into three zones (about 50 nm in diameter), *i.e.* I, II and III, and the corresponding SADPs are shown as insets. In region I where the fine structure is observed a clear halo pattern is seen in the corresponding SADP I, suggesting the existence of an amorphous phase (featureless image). In contrast, the structure in regions II and III shows fringe images corresponding to b.c.c. TaAl solid solution and h.c.p. TaN. We should emphasize that the h.c.p. TaN phase formed could not be detected by the XRD technique. This might be attributed to there being only a small fraction of h.c.p. TaN present in the alloy powders, which the resolution of our XRD apparatus is not powerful enough to identify. It is worth noting that no other nitride phase(s) could be detected.

The BFI and corresponding SADP of a near-edge particle taken after 86 ks of RBM are shown in Fig. 6d. Overall, the sample appears to have a homogeneous fine structure with no dominant facet structure. Moreover, the SADP shows a typical halo pattern of an amorphous phase in good agreement with the XRD pattern of Fig. 1.

The TEM technique allows us to determine the crystalline size of the the TaAlN alloy during the RBM process. These results are in fair agreement with the results of XRD (closed triangle symbols) using the Scherrer equation [32], as shown in Fig. 7. The grain size of the TaAlN decreases monotonically with increasing RBM time to become almost invisible after 55 ks, *i.e.* amorphous starting stage.

Figure 8 shows the HRTEM image and corresponding SADP for the as-annealed (1700 K) powder of the 86 ks TaAlN alloy. Obviously the annealed alloy powder contains several twins and nanotwins with fringe images of tetragonal crystalline TaAl and h.c.p. TaN. The SADP taken from several regions exhibits Debye–Scherrer rings of TaAl overlapped with TaN (small spots) (inset of Fig. 8).

3.3. Thermal analysis

Figure 9 shows typical DTA curves for TaAlN alloy powders as a function of the RBM time. All samples were heated to 1400 K (first run) and cooled to about 400 K. Then second heating runs (dashed curves) were performed in order to get a baseline. After 2 ks of RBM a sharp endothermic peak appears at about 930 K due to the melting of pure Al in the starting material of Ta and Al powders. The melt then reacts with elemental Ta powder in the mixture, as characterized by an exothermic peak appearing above 1200 K. After

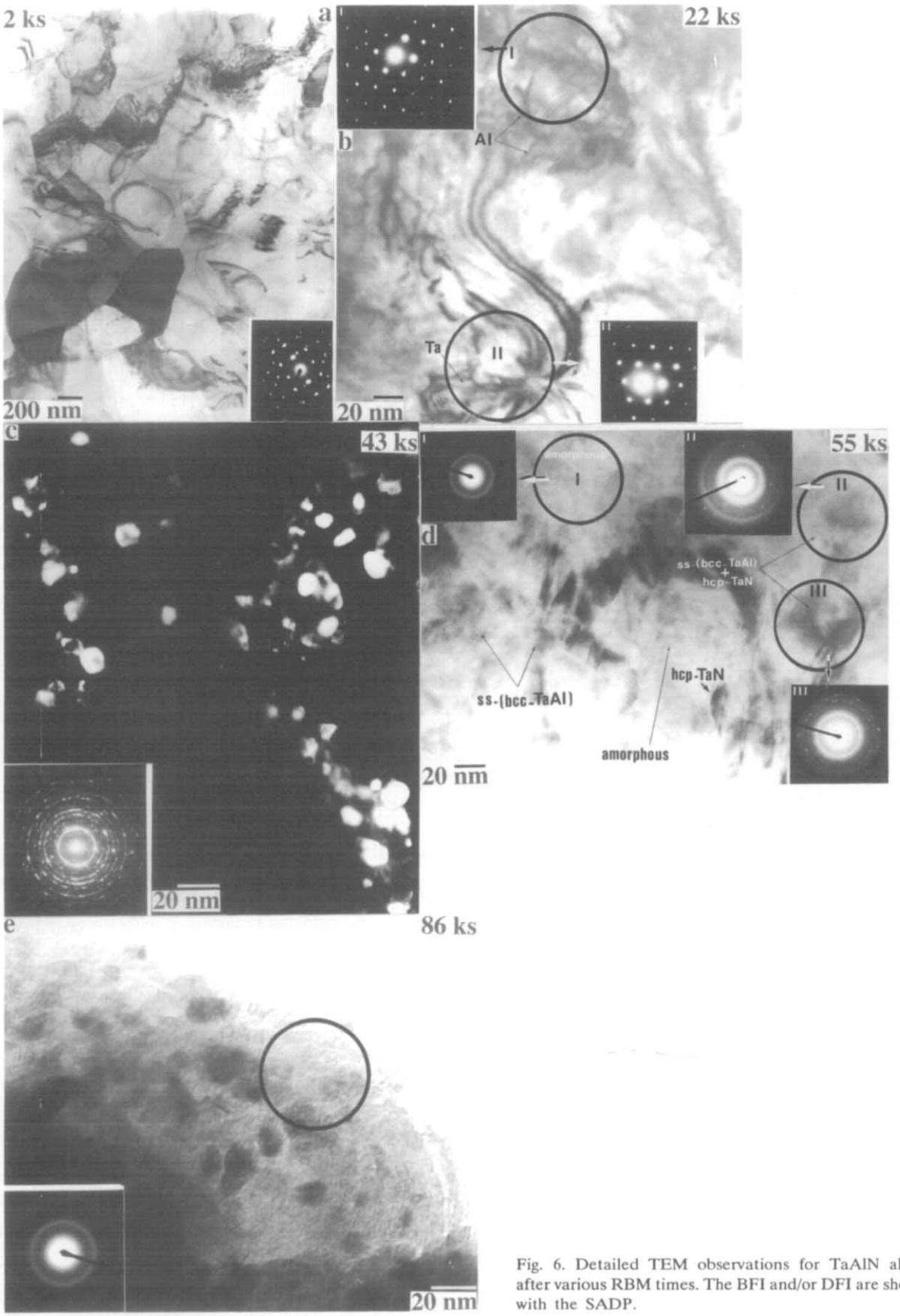

Fig. 6. Detailed TEM observations for TaAlN alloy powders after various RBM times. The BFI and/or DFI are shown together with the SADP.

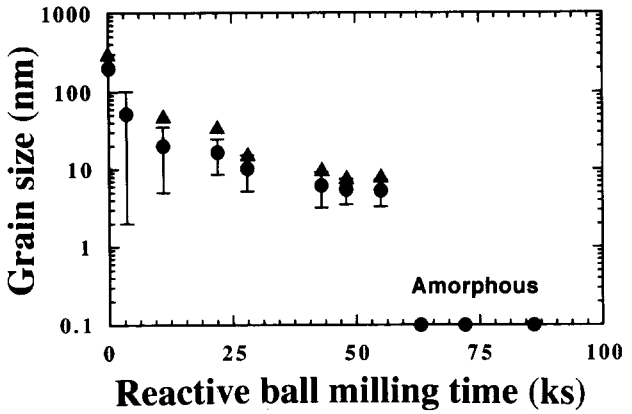

Fig. 7. Grain size distribution of $Ta_{50}Al_{50}$ alloy powders as a function of RBM time: ●, estimated from TEM observations; ▲, estimated from halfwidths of XRD lines using the Scherrer equation.

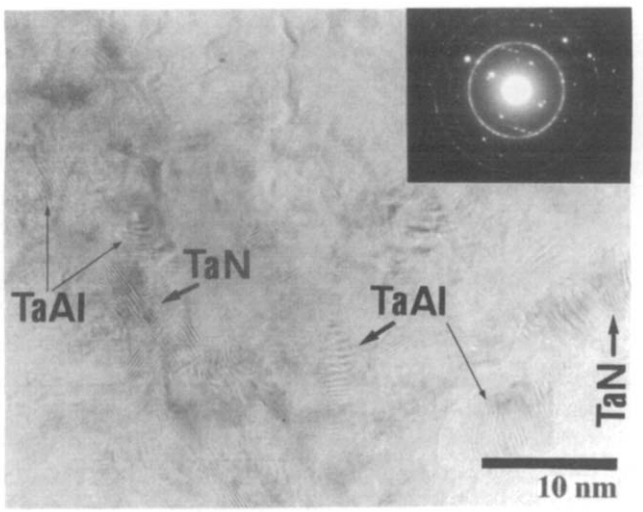

Fig. 8. HRTEM image of 86 ks TaAlN alloy powder heated to 1700 K.

11 ks of milling, however, the endothermic and exothermic reaction peaks have already disappeared and a single broad exothermic peak appears at low temperature. This peak is attributed to the crystallization of the amorphous phase in the alloy powders. It is worth noting that the peak temperature of this crystallization peak is shifted to a higher value at the intermediate stage (22–55 ks) of milling. Towards the end of the MA time (86 ks) the crystallization peak becomes pronounced and sharp, suggesting the formation of a homogeneous amorphous alloy.

The crystallization characteristics of amorphous TaAlN alloy powder indexed by the crystallization temperature T_x (temperature of crystallization peak) and the enthalpy change of crystallization, ΔH_x (the area under crystallization peak), are shown in Figs. 10 and 11 respectively. Obviously T_x increases drastically with increasing RBM time during the early and intermediate

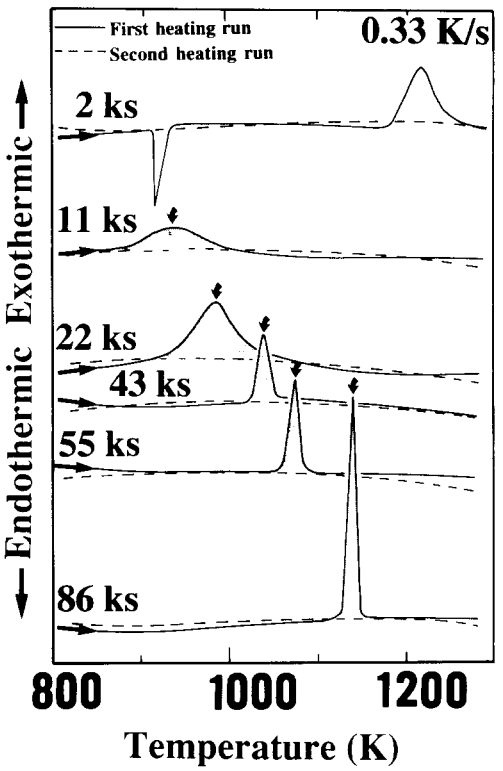

Fig. 9. Typical DTA curves for TaAlN alloy powders after various RBM times.

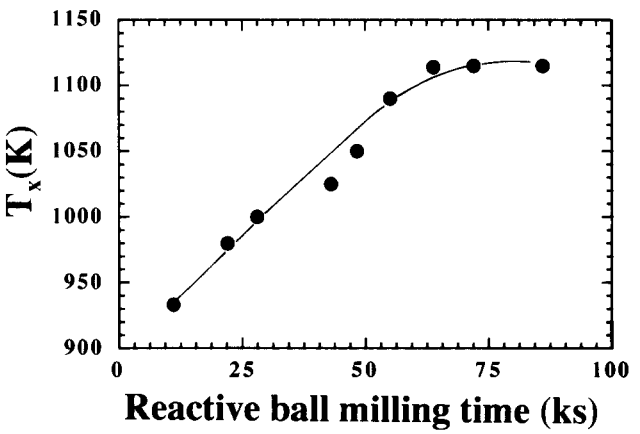

Fig. 10. Crystallization temperature T_x for TaAlN alloy powders as a function of RBM time.

stages of milling, indicating a continuous change in the composition of the amorphous phase, and approaches a saturation value of about 1115 K during the final stage of RBM (Fig. 10). The value of ΔH_x decreases monotonically with increasing RBM time, suggesting an increase in the mole fraction of the amorphous phase formed in the alloy powders. This value saturated at -95 kJ mol^{-1} after 55 ks of milling (Fig. 11).

3.4. Chemical analysis

Figure 12 displays the nitrogen content absorbed in mechanically alloyed TaAl powders as a function of

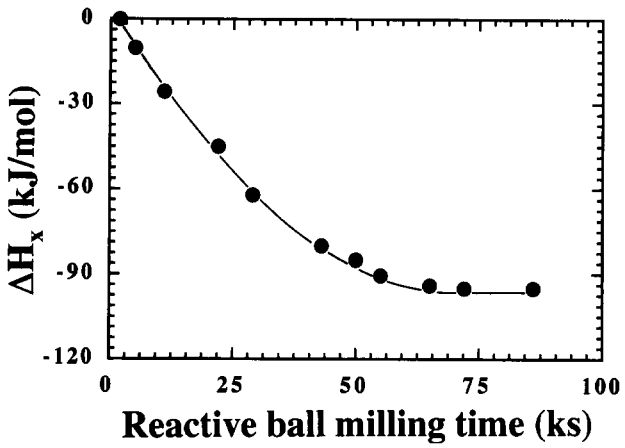

Fig. 11. Enthalpy change of crystallization, ΔH_x, for TaAlN alloy powders as a function of RBM time.

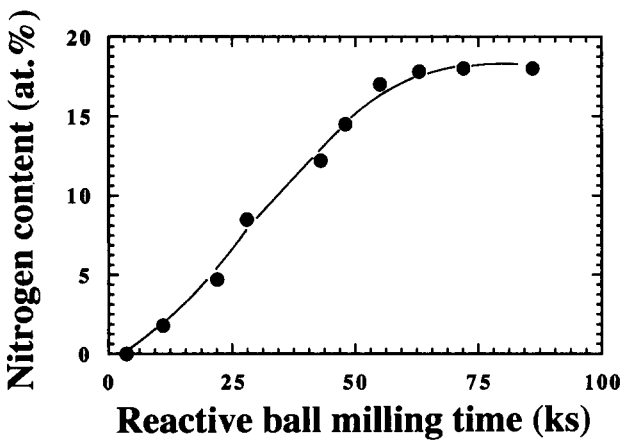

Fig. 12. Nitrogen content in TaAlN alloy powders as a function of RBM time.

the RBM time. During the early (0–22 ks) and intermediate (22–55 ks) stages of RBM the nitrogen content increases monotonically with increasing RBM time, suggesting a continuous reaction between the fresh surfaces of the powder particles and the fresh nitrogen gas flow. Towards the end of the RBM process, the nitrogen content in the milled TaAl powders saturated during the final stage of RBM (55–86 ks) at about 18 at.%.

4. Discussion

Mechanical alloying of elemental Ta and Al mixed powders under a nitrogen gas flow leads to the formation of TaAlN amorphous alloy powders. The results have shown that the so-called RBM process for producing amorphous TaAlN alloy can be classified mainly into three stages. The end-product of each stage varies widely in terms of structure, morphology, metallography and thermal proprieties. In this section we shall discuss the mechanism of the RBM process through each stage. Moreover, the role of amorphization and/or crystallization via each stage of milling will be discussed as well.

4.1. The early stage: the negative stage of milling

The early stage (0–22 ks) may be referred to as the first milling stage of the RBM process. During the first few kiloseconds of the RBM process, *e.g.* 2 ks, the powder particles of Ta and Al blend together without forming any composite particles. As a result of cold welding, almost all the starting material powders consist of assemblages or agglomerations of Ta and Al forming composite particles of larger diameter, as illustrated in Figs. 3a and 3b. This stage of milling can also be called the *negative milling stage*, in which the size of the powder particles increases. Thus the creation of new or fresh surfaces of the particles is absent. The nitrogen gas content in these powders is almost zero owing to the absence of fresh surfaces which enhance the solid–gas reaction (see Section 4.2), as was shown in Fig. 12. The particles at this stage of the RBM process have a well-developed lamellar structure of elemental Ta and Al, as was shown in Fig. 4a. During this stage there is no significant difference in thermal properties between the agglomerated powder particles and the starting materials, as was shown by the DTA measurements in Fig. 9. Therefore the process at the early stage has the appearance of just blending of the two elemental metal powders. Further, the composite particles formed vary significantly in composition from particle to particle, suggesting that the milling process at this stage produces a heterogeneous alloy powder containing b.c.c. TaAl solid solution coexisting with unprocessed powders of Ta and Al, as was shown in Figs. 6a and 6b.

4.2. The intermediate stage: The stage of solid–gas reaction accompanied by SSAR

The previous negative stage of milling is followed by a second stage which is called the intermediate stage or *positive stage of milling* (22–55 ks). Here the agglomerated particles are shattered and disintegrated into several particles apparently irregular in shape and size, as was shown in Fig. 3c. This disintegration of the powder particles has occurred as a result of a continuous shear stress and impact force generated by ball–powder–ball collisions. Because the powders are subjected to these external forces, new or fresh active surfaces of the particles appear.

At this stage of RBM all Bragg peaks of the f.c.c. Al crystals diffuse completely into the Bragg peaks of the b.c.c. Ta crystals, indicating the formation of a b.c.c. TaAl solid solution, as was displayed in Fig. 1. It is worth noting that the layered structure morphology,

as examined by cross-sectional view of the particles, has already disappeared, suggesting the formation of a single phase (b.c.c. TaAl solid solution), as was shown in Fig. 4b. The nitrogen content absorbed in this solid solution alloy powder increases monotonically with increasing RBM time, indicating the formation of a b.c.c. TaAl nitride. TEM as a powerful tool has shown that a small fraction of unprocessed b.c.c. Ta powder reacts with nitrogen gas to form h.c.p. TaN, precipitated in the matrix of b.c.c. TaAl nitride, as was shown in Fig. 6d. As the milling time increases to 43 ks, the b.c.c. solid solution expands to 0.3343 nm. In fact, this value is larger than that of pure crystalline b.c.c. Ta (0.3306 nm), suggesting an interstitial solubility of Al in Ta, as was illustrated in Fig. 2.

Based on a careful TEM analysis of the mechanically alloyed powders of this stage, there are two phases that react with each other, *i.e.* the b.c.c. TaAl nitride solid solution (main phase) and h.c.p. TaN (subphase) present in the milled powders. Further milling leads to mechanical deformations of the powders which give rise to various defects in the b.c.c. TaAl nitride solid solution. These defects are able to change the free energy of the solid solution to the less stable phase of amorphous TaAlN. In addition, the small fraction of h.c.p. TaN reacts with the formed amorphous phase in a heterogeneous reaction so that an amorphous phase of TaAlN with a nitrogen concentration of about 18 at.% is formed at the end of this stage. The reaction between the above-mentioned phases seems to take place in the same manner as reported earlier by Lee and Koch [33] for the reaction between two intermetallic compounds. More recently, Aoki *et al.* [34] have reported that an amorphous phase of NiZrN can also be formed as a result of amorphization between several phases, *i.e.* ZrN, Ni, Zr and amorphous $NiZrN_x$, using the MA technique under a nitrogen atmosphere.

During this stage, the amorphous alloy crystallizes and this is accompanied by a rather broad exothermic peak due to the heterogeneity of the amorphous phase formed, as was shown in Fig. 9. Moreover, both T_x and $-\Delta H_x$ increase monotonically, suggesting a continuous compositional change and an increase in the volume fraction of amorphous TaAlN alloy in the milled powders respectively.

4.3. The final stage: The homogenization stage

In the present study we shall define the final stage of the RBM process (55–86 ks) as the *homogenization stage*, in which the SSAR takes place homogeneously and a uniform amorphous phase of TaAlN is obtained. Towards the end of this stage the TaAlN amorphous phase gives XRD patterns with broad and smooth peaks, as was shown in Fig. 1. In addition, the amorphous alloy powders crystallize through a single sharp exothermic peak (Fig. 9), suggesting that the amorphous phase formed is single phase and homogeneous in composition. In fact, the amorphous phase formed at this stage is more homogeneous than that of the previous stage. This is demonstrated by the nearly constant values of the particle size, grain size, T_x and ΔH_x. Heating the amorphous phase of TaAlN to 1700 K leads to the formation of a crystalline mixture of tetragonal TaAl and h.c.p. TaN phases, as illustrated in Fig. 8.

5. Conclusions

New amorphous TaAlN alloy has been fabricated by milling an equiatomic mixture of elemental Ta and Al powders in a high energy ball mill under a purified nitrogen gas flow at room temperature. In the present study we have classified the RBM process through three stages of milling, the end-product differing widely from stage to stage. During the first stage the elemental powders of Ta and Al particles form layered composite particles of larger diameter as a result of cold welding. In the second stage the elemental Al powder particles have been completely diffused into the Ta matrix to form a b.c.c. TaAl solid solution. This solid solution expands with increasing milling time and leads to a saturation value in the lattice parameter a_0, of 0.3306 nm after 55 ks of milling. During this stage the powders disintegrate into several particles which have fresh surfaces that can absorb nitrogen gas, so that both the b.c.c. TaAl solid solution and the unprocessed b.c.c. Ta powder particles react with nitrogen to form a b.c.c. TaAl solid solution nitride and h.c.p. TaN respectively. Further mechanical deformations that result from increasing the RBM time lead to a transformation of the nitride phase of the b.c.c. TaAl solid solution into the less stable phase of amorphous TaAlN. A homogeneous phase of amorphous TaAlN is formed containing 18 at.% N_2 after 72 ks of RBM. The crystallization characteristics represented by the crystallization temperature T_x and the enthalpy change of crystallization, ΔH_x, are 1115 K and -95 kJ mol^{-1} respectively.

Acknowledgments

The author is indebted to Professor K. Suzuki and Professor K. Aoki of the Institute for Materials Research, Tohoku University, Sendai, Japan for helpful discussions.

References

1 J.S. Benjamin, *Metall. Trans. A, 1* (1970) 2943.
2 I.G. Wright and A. Wilox, *Metall. Trans. A, 5* (1974) 957.
3 G.H. Gessinger, *Metall. Trans. A, 1* (1976) 1203.
4 J.S. Benjamin, *Sci. Am., 40* (1976) 234.
5 C.C. Koch, O.B. Cavin, C.G. McKamey and J.O. Scarbourgh, *Appl. Phys. Lett., 43* (1983) 1017.
6 R.B. Schwarz and W.L. Johnson, *Phys. Rev. Lett., 51* (1983) 415.
7 A.E. Ermakov, E.E. Yurchikov and V.A. Barinov, *Phys. Met. Metall., 52* (1981) 50.
8 M. Sherif El-Eskandarany, K. Aoki and K. Suzuki, *J. Alloys Comp., 177* (1991) 229.
9 M. Sherif El-Eskandarany, F. Itoh, K. Aoki and K. Suzuki, *J. Non-Cryst. Solids, 117–118* (1990) 729.
10 E. Hellstern, L. Schultz, R. Bormann and D. Lee, *Appl. Phys. Lett., 53* (1988) 1399.
11 M. Sherif El-Eskandarany, K. Aoki and K. Suzuki, *Scr. Metall., 25* (1991) 1695.
12 E. Gaffet and M. Harmelin, *J. Phys. (Paris), Colloq. C4, Suppl. 14, 51* (1990) 139.
13 E. Gaffet, C. Louison, M. Harmelin and F. Faudot, *Mater. Sci. Eng. A, 134* (1991) 1380.
14 E. Gaffet and M. Harmelin, *J. Less-Common Met., 157* (1990) 201.
15 M. Sherif El-Eskandarany, K. Aoki and K. Suzuki, *J. Less-Common Met., 167* (1990) 113.
16 M. Sherif El-Eskandarany, K. Aoki and K. Suzuki, *J. Non-Cryst. Solids, 150* (1992) 472.
17 M. Sherif El-Eskandarany, K. Aoki and K. Suzuki, *Metall. Trans. A, 23* (1992) 2131.
18 M. Sherif El-Eskandarany, K. Aoki and K. Suzuki, *J. Appl. Phys., 71*(6) (1992) 2924.
19 M. Sherif El-Eskandarany, K. Aoki and K. Suzuki, *Mater. Sci. Forum, 88–90* (1992) 81.
20 M. Sherif El-Eskandarany, K. Aoki and K. Suzuki, *J. Appl. Phys., 72*(7) (1992) 2665.
21 M. Sherif El-Eskandarany, K. Aoki and K. Suzuki, *J. Alloys Comp., 186* (1992) 15.
22 M. Sherif El-Eskandarany, K. Aoki and K. Suzuki, *J. Non-Cryst. Solids, 150* (1992) 472.
23 C. Politis and W.L. Johnson, *J. Appl. Phys., 60* (1986) 1147.
24 R.B. Schwarz and R.R. Petrich, *J. Less-Common Met., 140* (1988) 171.
25 J.S.C. Jang and C.C. Koch, *J. Mater. Res., 5* (1990) 498.
26 M. Sherif El-Eskandarany, K. Aoki, H. Itoh and K. Suzuki, *J. Less-Common Met., 169* (1991) 235.
27 K.-J. Kim, M. Sherif El-Eskandarany, K. Sumiyama and K. Suzuki, *J. Non-Cryst. Solids, 155* (1993) 165.
28 M. Sherif El-Eskandarany, K. Sumiyama, K. Aoki and K. Suzuki, *J. Mater. Res., 7*(4) (1992) 888.
29 M. Sherif El-Eskandarany, K. Aoki and K. Suzuki, *Mater. Sci. Forum, 88–90* (1992) 801.
30 M. Sherif El-Eskandarany, K. Aoki and K. Suzuki, *Appl. Phys. Lett., 60*(13) (1992) 1562.
31 M. Sherif El-Eskandarany, K. Sumiyama, K. Aoki, T. Matsumoto and K. Suzuki, *J. Mater. Res.*, in press.
32 A. Guinier, *X-Ray Diffraction,* Freeman, San Francisco, CA, 1963, p. 124.
33 P.Y. Lee and C.C. Koch, *Appl. Phys. Lett., 50* (1987) 1578.
34 K. Aoki, A. Memezawa and T. Matsumoto, *J. Mater. Res., 8* (1993) 307.